FLORE
Repository istituzionale dell'Università degli Studi di Firenze

A generalized definition of Power Gain Taking Harmonic Content into Account

(Article begins on next page)

10 January 2022

Expanding Definitions of Gain by Taking Harmonic Content into Account

Jeffrey Jargon,[1] K. C. Gupta,[2] Alessandro Cidronali,[3] Donald DeGroot[1]

[1] National Institute of Standards and Technology 325 Broadway, M/S 813.01,
Boulder, Colorado 80305
[2] University of Colorado at Boulder, Boulder, Colorado 80309
[3] University of Florence, 50139 Florence, Italy

ABSTRACT: We expand the definitions of power gain, transducer gain, and available gain by taking harmonic content into account. Furthermore, we show that under special conditions, these expanded definitions of gain can be expressed in terms of nonlinear large-signal scattering parameters. Finally, we provide an example showing how these expanded forms of gain and nonlinear large-signal scattering parameters can provide us with valuable information regarding the behavior of nonlinear models. © 2003 Wiley Periodicals, Inc. Int J RF and Microwave CAE 13: 357–369, 2003.*

I. INTRODUCTION

Three types of gain are commonly used as figures of merit for two-port networks — power gain, transducer gain, and available gain [1]. Power gain G is defined as the ratio of the power delivered to the load P_L connected at port 2 of the device to the input power P_{IN} at port 1 of the device

$$G \equiv \frac{P_L}{P_{IN}}, \qquad (1)$$

where P_L and P_{IN} can be described in terms of wave variables referenced to some real-valued impedance

$$P_{IN} = \tfrac{1}{2} |a_1|^2 - \tfrac{1}{2} |b_1|^2 \qquad (2)$$

and

$$P_L = \tfrac{1}{2} |b_2|^2 - \tfrac{1}{2} |a_2|^2. \qquad (3)$$

Here, a_i and b_i refer to the complex incident and reflected power-normalized waves, respectively, where the subscript i denotes the port number. Transducer gain G_T is defined as the ratio of the power delivered to the load P_L to the power available from the source P_{AVS}:

$$G_T \equiv \frac{P_L}{P_{AVS}}. \qquad (4)$$

The power available from the source P_{AVS} is the maximum power that can be delivered to the network. This occurs when the input impedance of the terminated network is conjugate matched to the source impedance, and can be described in terms of power-normalized waves as

$$P_{AVS} = P_{IN}\big|_{\Gamma_{IN}=\Gamma_S^*} = \tfrac{1}{2} |a_1|^2. \qquad (5)$$

Available gain G_A is defined as the ratio of the power available from the network P_{AVN} to the power available from the source P_{AVS}:

$$G_A \equiv \frac{P_{AVN}}{P_{AVS}}. \qquad (6)$$

The power available from the network P_{AVN} is the maximum power that can be delivered to the load. This occurs when the output impedance of the terminated network is conjugate matched to the load impedance, and can be described in terms of power-normalized waves as

$$P_{AVN} = P_L|_{\Gamma_L = \Gamma_{OUT}^*} = \tfrac{1}{2} |b_2|^2. \qquad (7)$$

One limitation of the gain definitions described in eqs. (1), (4), and (6) is that they are restricted to the fundamental operating frequency, and thus do not take into account energy at higher harmonic frequencies.

In this article, we expand the definitions of power gain, transducer gain, and available gain by taking harmonic content into account. Furthermore, we show that under special conditions, these expanded forms of gain can be expressed in terms of nonlinear large-signal scattering parameters, previously introduced in [2–4]. Together, these figures of merit can be used to discover valuable information regarding the behavior of nonlinear models. Specifically, we will examine a lumped-element model of a pseudomorphic high-electron-mobility transistor (pHEMT) device operating in a two-port, common-source configuration. First, we will look at the nonlinear large-signal scattering parameters as a function of power for various bias conditions, and then we will reduce the scattering parameter data set by calculating the expanded power gain $\mathfrak{G}$, the expanded transducer gain $\mathfrak{G}_T$, and the ratio of the power gain confined to the excitation frequency to that of the overall power gain $\mathfrak{G}_1/\mathfrak{G}$.

II. EXPANDED DEFINITIONS OF GAIN

In the case of a sinusoidal input to a two-port nonlinear device, power may be transferred to higher harmonic frequencies. Thus, we can modify the definitions of power, described in the previous section by taking into account the harmonic contributions and summing over all K harmonics considered. First, the input power P_{IN} given in eq. (2) can be modified to

$$P_{IN} = \frac{1}{2} \sum_{k=1}^{K} |a_{1k}|^2 - \frac{1}{2} \sum_{k=1}^{K} |b_{1k}|^2. \qquad (8)$$

Here, a_{ik} and b_{ik} refer to the complex incident and reflected power-normalized waves, respectively, where the subscript i denotes the port number and k denotes the spectral component number. All waves must be taken with respect to a real-valued, reference impedance. Similarly, we can modify the other definitions as follows:

$$P_L = \frac{1}{2} \sum_{k=1}^{K} |b_{2k}|^2 - \frac{1}{2} \sum_{k=1}^{K} |a_{2k}|^2, \qquad (9)$$

$$P_{AVS} = \frac{1}{2} \sum_{k=1}^{K} |a_{1k}|^2, \qquad (10)$$

and

$$P_{AVN} = \frac{1}{2} \sum_{k=1}^{K} |b_{2k}|^2. \qquad (11)$$

Eqs. (8–11) are valid under the assumption that the power in the network is confined to a grid of frequencies that are harmonically related.

Once again, the expanded power gain $\mathfrak{G}$ is defined as the ratio of P_L to P_{IN} and is given by

$$\mathfrak{G} \equiv \frac{P_L}{P_{IN}} = \frac{\frac{1}{2} \sum_{k=1}^{K} |b_{2k}|^2 - \frac{1}{2} \sum_{k=1}^{K} |a_{2k}|^2}{\frac{1}{2} \sum_{k=1}^{K} |a_{1k}|^2 - \frac{1}{2} \sum_{k=1}^{K} |b_{1k}|^2}, \qquad (12)$$

the expanded transducer gain $\mathfrak{G}_T$ is defined as the ratio of P_L to P_{AVS} and is given by

$$\mathfrak{G}_T \equiv \frac{P_L}{P_{AVS}} = \frac{\frac{1}{2} \sum_{k=1}^{K} |b_{2k}|^2 - \frac{1}{2} \sum_{k=1}^{K} |a_{2k}|^2}{\frac{1}{2} \sum_{k=1}^{K} |a_{1k}|^2}, \qquad (13)$$

and the expanded available gain $\mathfrak{G}_A$ is defined as the ratio of P_{AVN} to P_{AVS} and is given by

$$\mathfrak{G}_A \equiv \frac{P_{AVN}}{P_{AVS}} = \frac{\frac{1}{2} \sum_{k=1}^{K} |b_{2k}|^2}{\frac{1}{2} \sum_{k=1}^{K} |a_{1k}|^2}. \qquad (14)$$

III. EXPANDED DEFINITIONS OF GAIN IN TERMS OF NONLINEAR LARGE-SIGNAL SCATTERING PARAMETERS

In previous work [2–4], we introduced the concept of nonlinear large-signal scattering parameters. Like commonly used linear *S*-parameters, nonlinear large-signal $\mathfrak{S}$-parameters can also be expressed as ratios of incident and reflected wave variables. However, unlike linear *S*-parameters, nonlinear large-signal $\mathfrak{S}$-parameters depend upon the signal magnitude and must take into account the harmonic content of the input and output signals since energy can be transferred to other frequencies in a nonlinear device.

For simplicity, we consider a two-port device excited at port 1 by a single-tone signal (a_{11}) at a frequency f_1. This condition is commonly encountered with power amplifiers and frequency doublers, although the approach can be generalized to any number of ports with multiple excitations that are harmonically related. In this case, we extract an input reflection coefficient, given by

$$\mathfrak{S}_{11k1} = \frac{|b_{1k}|}{|a_{11}|} \angle (\phi_{b_{1k}} - k\phi_{a_{11}})\big|_{a_{mn}=0 \text{ for } \forall m \forall n[(m\neq1)\wedge(n\neq1)]},$$

(15)

where a_{jl} (port *j*, spectral component number *l*) and b_{ik} (port *i*, spectral component number *k*) refer to the complex incident and scattered power-normalized waves, respectively, and $\mathfrak{S}_{ijkl}$ indicates the nonlinear large-signal $\mathfrak{S}$-parameter. Note that while taking the ratio of b_{ik} to a_{11}, we set the phase reference to (a_{11}). Using the method of [4] to accomplish this, we subtract *k* times the phase of (a_{11}) from that of b_{ik}, since the phases are in terms of their respective frequencies. Note that all phases φ are in units of degrees and have a modulus of 360° (i.e., $0° \leq \varphi < 360°$). The additional limitation imposed on eq. (15) is that all other incident waves other than a_{11} equal zero. Another valuable parameter, the forward transmission coefficient, is similarly extracted as

$$\mathfrak{S}_{21k1} = \frac{|b_{2k}|}{|a_{11}|} \angle (\phi_{b_{2k}} - k\phi_{a_{11}})\big|_{a_{mn}=0 \text{ for } \forall m \forall n[(m\neq1)\wedge(n\neq1)]}.$$

(16)

This parameter provides the designer with a value of the gain or loss through a device, either at the fundamental frequency, or converted to a higher harmonic frequency. Once again, we set the phase reference to

a_{11} and impose the limitation that all incident waves other than a_{11} equal zero.

When we extract the nonlinear large-signal scattering parameters $\mathfrak{S}_{11k1}$ and $\mathfrak{S}_{21k1}$, described in eqs. (15) and (16), only a_{11} is present and all other a's are forced to zero. In this case, eq. (8) is reduced to

$$P_{IN} = \frac{1}{2}|a_{11}|^2 - \frac{1}{2}\sum_{k=1}^{K}|b_{1k}|^2.$$

(17)

Likewise, eq. (9) becomes

$$P_L = \frac{1}{2}\sum_{k=1}^{K}|b_{2k}|^2,$$

(18)

and eq. (10) simplifies to

$$P_{AVS} = \frac{1}{2}|a_{11}|^2.$$

(19)

Eq. (11), however, remains unchanged as

$$P_{AVN} = \frac{1}{2}\sum_{k=1}^{K}|b_{2k}|^2,$$

(20)

since it contains no a_{ij} terms.

In this case, only a_{11} is present and all other a's are forced to zero, so that the expanded power gain $\mathfrak{G}$ can be expressed as

$$\mathfrak{G} \equiv \frac{P_L}{P_{IN}} = \frac{\frac{1}{2}\sum_{k=1}^{K}|b_{2k}|^2}{\frac{1}{2}|a_{11}|^2 - \frac{1}{2}\sum_{k=1}^{K}|b_{1k}|^2}.$$

(21)

Dividing both the numerator and denominator of eq. (21) by $|a_{11}|^2$, and substituting in eqs. (15) and (16) gives the power gain in terms of the nonlinear large-signal scattering parameters:

$$\mathfrak{G} = \frac{\sum_{k=1}^{K}|\mathfrak{S}_{21k1}|^2}{1 - \sum_{k=1}^{K}|\mathfrak{S}_{11k1}|^2}.$$

(22)

The power gain confined to the nth harmonic frequency is
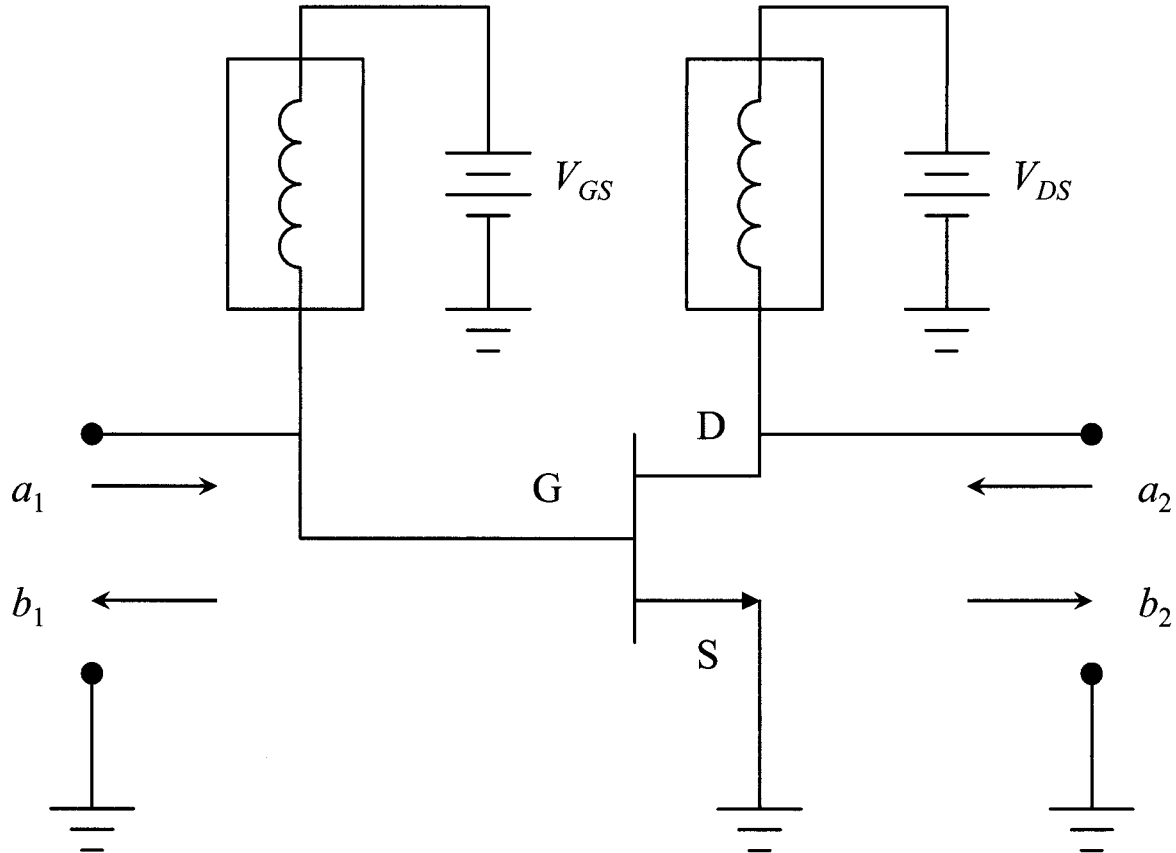
Figure 1. Circuit diagram of a pHEMT device operating in a two-port, common-source configuration.

$$\mathfrak{G}_n = \frac{|\mathfrak{S}_{21n1}|^2}{1 - \Sigma_{k=1}^{K} |\mathfrak{S}_{11k1}|^2}. \tag{23}$$

The ratio $\mathfrak{G}_n/\mathfrak{G}$ expresses the fraction of the power gain confined to the nth harmonic frequency compared to the power gain over all of the harmonic frequencies considered.

Likewise, we can express the expanded transducer gain and expanded available gain in terms of nonlinear large-signal scattering parameters. With only a_{11} present and all other a's forced to zero, $\mathfrak{G}_T$ and $\mathfrak{G}_A$ reduce to the same expression:

$$\mathfrak{G}_T = \mathfrak{G}_A = \sum_{k=1}^{K} |\mathfrak{S}_{21k1}|^2. \tag{24}$$

Here, the transducer, or available, gain confined to the nth harmonic frequency is

$$\mathfrak{G}_{Tn} = \mathfrak{G}_{An} = |\mathfrak{S}_{21n1}|^2. \tag{25}$$

Once again, the ratio $\mathfrak{G}_{Tn}/\mathfrak{G}_T$, or $\mathfrak{G}_{An}/\mathfrak{G}_A$, expresses the fraction of the transducer, or available, gain confined to the nth harmonic frequency compared to the transducer, or available, gain over all of the harmonic frequencies considered. Note that $\mathfrak{G}_n/\mathfrak{G} = \mathfrak{G}_{Tn}/\mathfrak{G}_T = \mathfrak{G}_{An}/\mathfrak{G}_A$.

IV. EXAMPLE

Here, we provide an example showing how nonlinear large-signal scattering parameters along with the expanded definitions of gain, introduced in the previous section, can be used to discover valuable information regarding the behavior of a nonlinear model. Specifically, we examine a lumped-element model of a 2 × 90 μm GaAs pseudomorphic high electron mobility transistor (pHEMT) device operating in a two-port, common-source configuration, shown in Figure 1. The pHEMT model was developed by Cidronali et al. [5, 6] using S-parameter measurements and electromagnetic simulations of the device layout.

First, we will look at $\mathfrak{S}_{11k1}$ and $\mathfrak{S}_{21k1}$ as a function of power for various bias conditions, and then we will reduce the $\mathfrak{S}$-parameter data set by calculating the power gain $\mathfrak{G}$, the transducer gain, $\mathfrak{G}_T$, and the ratio of the power gain confined to the first harmonic to that of the overall power gain $\mathfrak{G}_1/\mathfrak{G}$. We examine the model operating at a frequency of 5 GHz and powers ranging from a small-signal level of -20 dBm to a level of 10 dBm, which is close to the maximum device rating. Since the model is valid for an *n*-channel device, the drain is biased positively with respect to the common source. In this case, we choose $V_{DS} = 3$ V. The gate is biased negatively with respect to the source since this condition controls the width of the depletion region and blocks part of the conducting channel region. Here, we vary V_{GS} from 0.0 V to -1.2 V in steps of 0.2 V.

We can easily determine the two-port, nonlinear large-signal scattering parameters, described in eqs. (7) and (8), as a function of power and bias using a commercial harmonic balance simulator with all *a*'s other than a_{11} forced to zero. Figure 2 plots the magnitudes of $\mathfrak{S}_{11k1}$ for the first four harmonics ($k = 1, 2, 3,$ and 4). We see that $|\mathfrak{S}_{1111}|$ remains relatively flat at all bias conditions with varying input power $|a_{11}|$. The value of $|\mathfrak{S}_{1111}|$ decreases as V_{GS} decreases from 0 V to -0.2 V, reaches a minimum of -2.325 dB at $V_{GS} = -0.2$ V, and then increases as V_{GS} is further decreased from -0.2 V to -1.0 V. The parameters $|\mathfrak{S}_{1121}|$, $|\mathfrak{S}_{1131}|$, and $|\mathfrak{S}_{1141}|$ generally increase with input power at all bias conditions. This reveals that as the input power is increased, more energy is converted to higher harmonic frequencies and appears at port 1.

Figure 3 plots the magnitudes of $\mathfrak{S}_{21k1}$ for the first four harmonics ($k = 1, 2, 3,$ and 4). At small input signals, $|\mathfrak{S}_{2111}|$ increases as V_{GS} decreases from 0 V to -0.4 V, reaches a maximum of 15.481 dB at $V_{GS} = -0.4$ V, and then decreases as V_{GS} is further decreased from -0.4 V to -1.0 V. The parameter $|\mathfrak{S}_{2111}|$ remains relatively flat and then gradually decreases with increasing $|a_{11}|$ for values of V_{GS} from 0 V to -0.6 V. At V_{GS} less than -0.6 V, $|\mathfrak{S}_{2111}|$ actually increases with increasing $|a_{11}|$ due to self-biasing. We also see that $|\mathfrak{S}_{2121}|$, $|\mathfrak{S}_{2131}|$, and $|\mathfrak{S}_{2141}|$ generally increase with input power at all bias conditions. This reveals that as the input power is increased, some of the energy converted to higher harmonic frequencies appears at port 2.

Since the nonlinear large-signal scattering parameters are complex quantities, the phase data are also plotted in Figure 4 for $V_{GS} = 0.0, -0.4,$ and -1.0 V.

To gain some physical insight into the pHEMT model, we can examine the nonlinear large-signal $\mathfrak{S}$-parameter data near pinch-off ($V_{GS} = -1.0$ V and $V_{DS} = 3$ V) and near $I_{DS} = I_{DSS}$ ($V_{GS} = 0$ V and $V_{DS} = 3$ V). In these two regions, the second harmonic content is maximum ($\mathfrak{S}_{2121} > \mathfrak{S}_{21k1}$ for $k > 2$), which can be seen in Figure 3. Near the pinch-off region, the device draws current only for the positive part of the gate voltage waveform, which results in a clamped waveform drain current, while near $I_{DS} = I_{DSS}$, the device saturates at the positive part of the gate voltage waveform and the device draws current only for the negative portion. Thus, taking the Fourier transform gives even harmonics of the same amplitude in both cases, but they are 180° out of phase. From Figure 4, we can see that near pinch-off ($V_{GS} = -1.0$ V), the phase of $\mathfrak{S}_{2121}$ is approximately 160°, while near $I_{DS} = I_{DSS}$ ($V_{GS} = 0$ V), the phase of $\mathfrak{S}_{2121}$ is approximately $-50°$. The difference in phase is about 210°, which is close to the expected value of 180°.

An additional benefit of examining the nonlinear large-signal $\mathfrak{S}$-parameters of a device is that having both the magnitude and phase of the harmonics is critical in the design of high-efficiency amplifiers and frequency multipliers.

Rather than looking at numerous graphs of nonlinear large-signal scattering parameters, we can get a more concise view of the modeled behavior of a device by reducing the nonlinear large-signal $\mathfrak{S}$-parameter data set into the compact expression of power gain $\mathfrak{G}$. Figure 5 plots the calculated values of $\mathfrak{G}$ using eq. (22) for $K = 4$, as a function of power for V_{GS} varying from 0.0 V to -1.2 V. At small signals, the power gain increases as V_{GS} decreases from 0 V to -0.4 V. The power gain reaches a maximum of 19.72 dB at $V_{GS} = -0.4$ V, and then decreases as V_{GS} is further decreased from -0.4 V to -1.2 V. This is consistent with the fact that the trans-conductance g_m, which is proportional to Y_{21} and hence S_{21}, peaks at a bias of $V_{GS} = -0.4$ V. We can also see from Figure 5 that the gain stays relatively flat and then gradually decreases with increasing $|a_{11}|$ for values of V_{GS} from 0 V to -0.6 V. At V_{GS} less than -0.6 V, the gain increases with increasing $|a_{11}|$ due to self-biasing and harmonic production.

We can also reduce the nonlinear large-signal $\mathfrak{S}$-parameter data set by using the compact expression of transducer gain $\mathfrak{G}_T$. Figure 6 plots the calculated values of $\mathfrak{G}_T$ using eq. (24) for $K = 4$, as a function of power for V_{GS} varying from 0.0 V to -1.2 V. At small signals, the power gain increases as V_{GS} decreases from 0 V to -0.4 V. The transducer gain
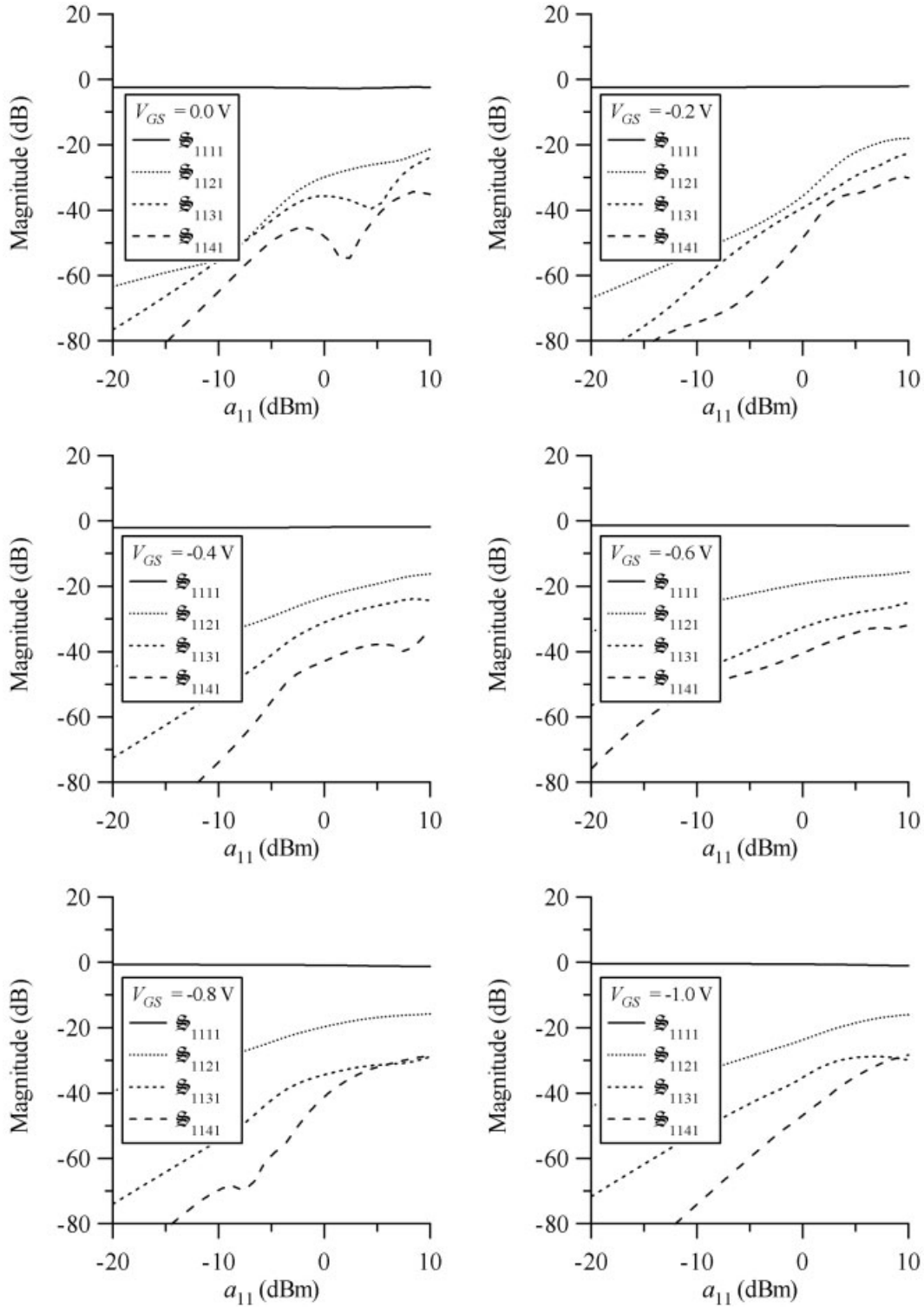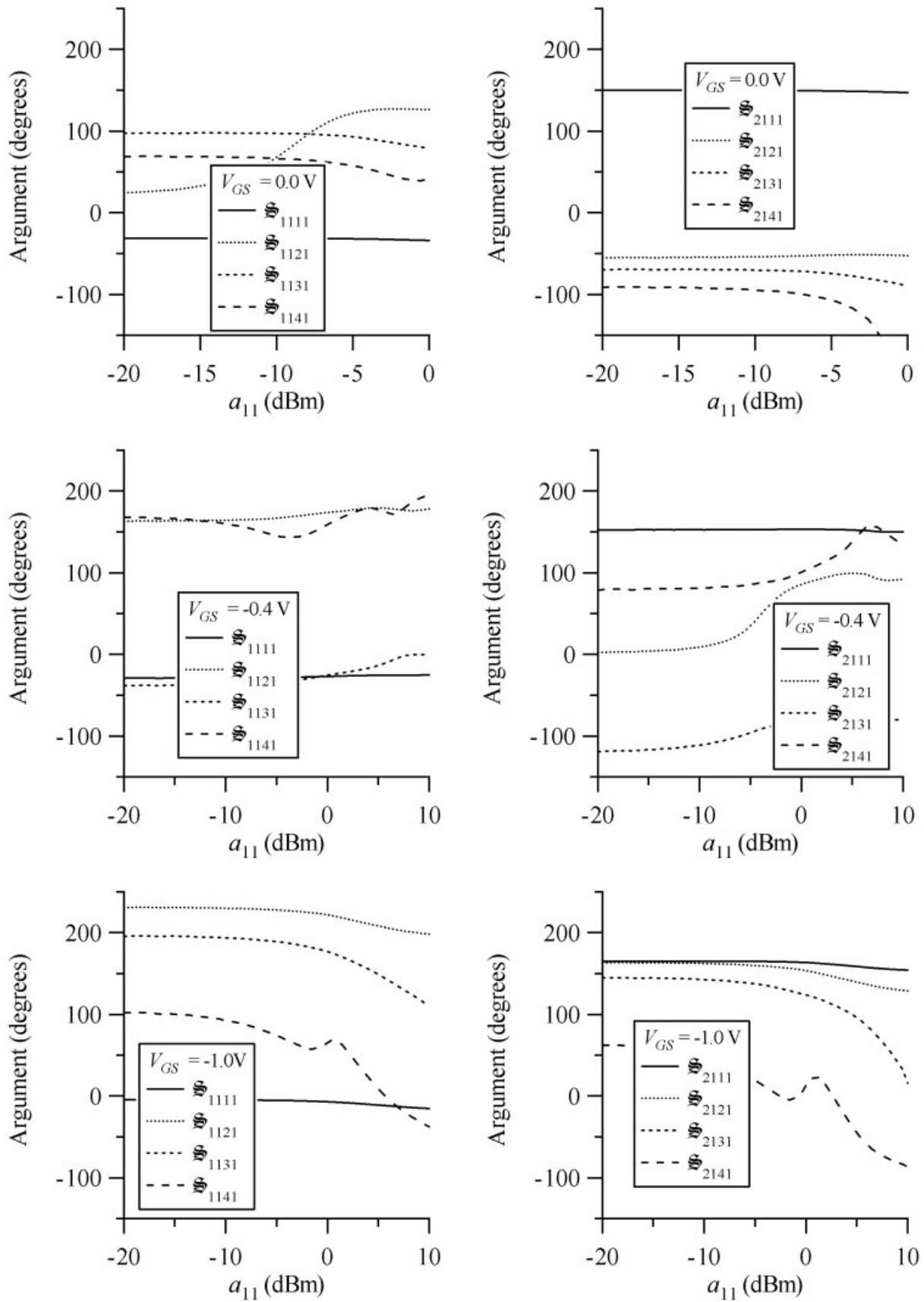
Figure 2. Magnitude of $\mathfrak{S}_{11k1}$ as a function of input power for a nonlinear lumped-element model of a 2×90 μm GaAs pHEMT device operating at 5 GHz and a bias of $V_{DS} = 3$ V and $V_{GS} = 0.0$, -0.2, -0.4, -0.6, -0.8, and -1.0 V.
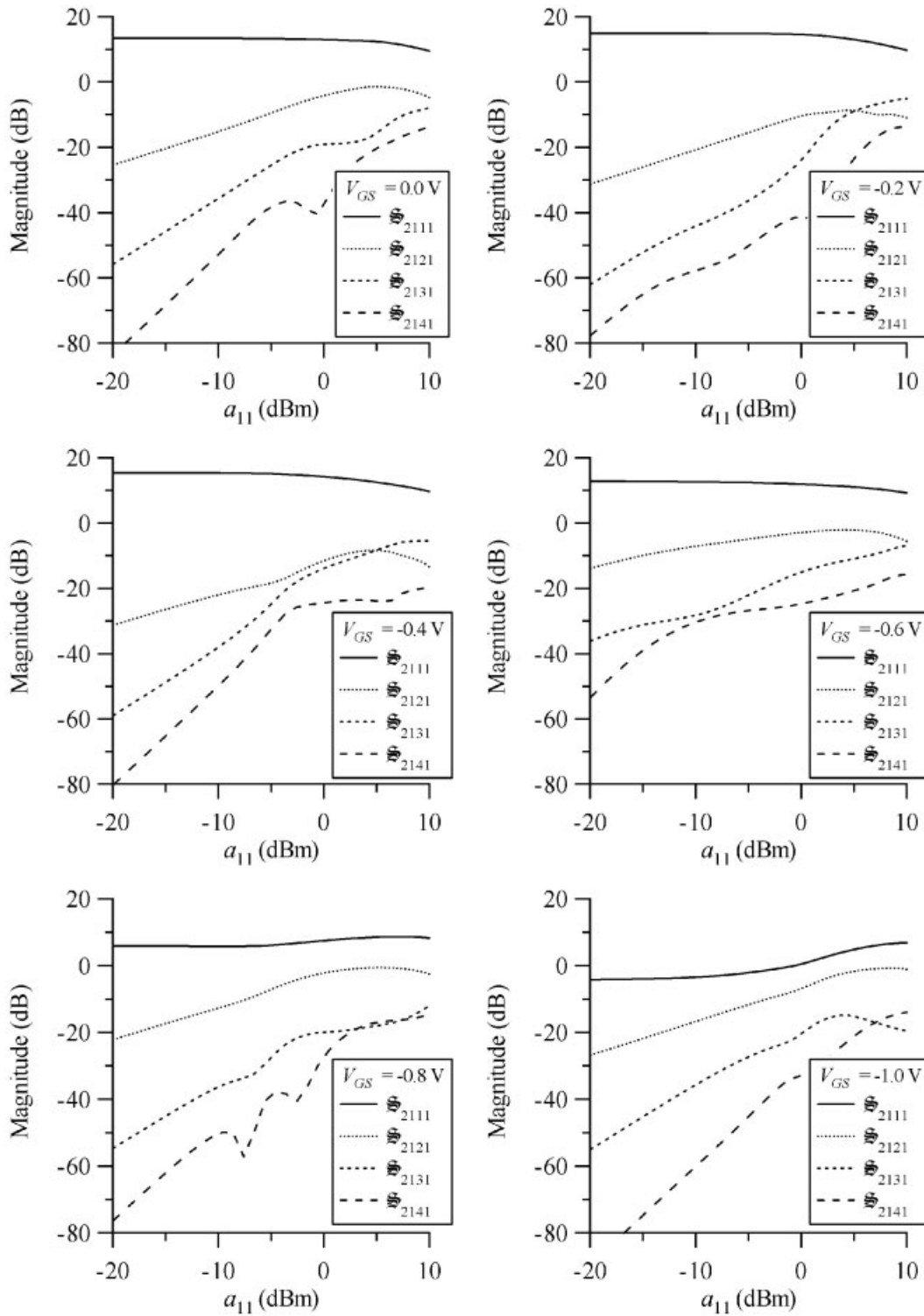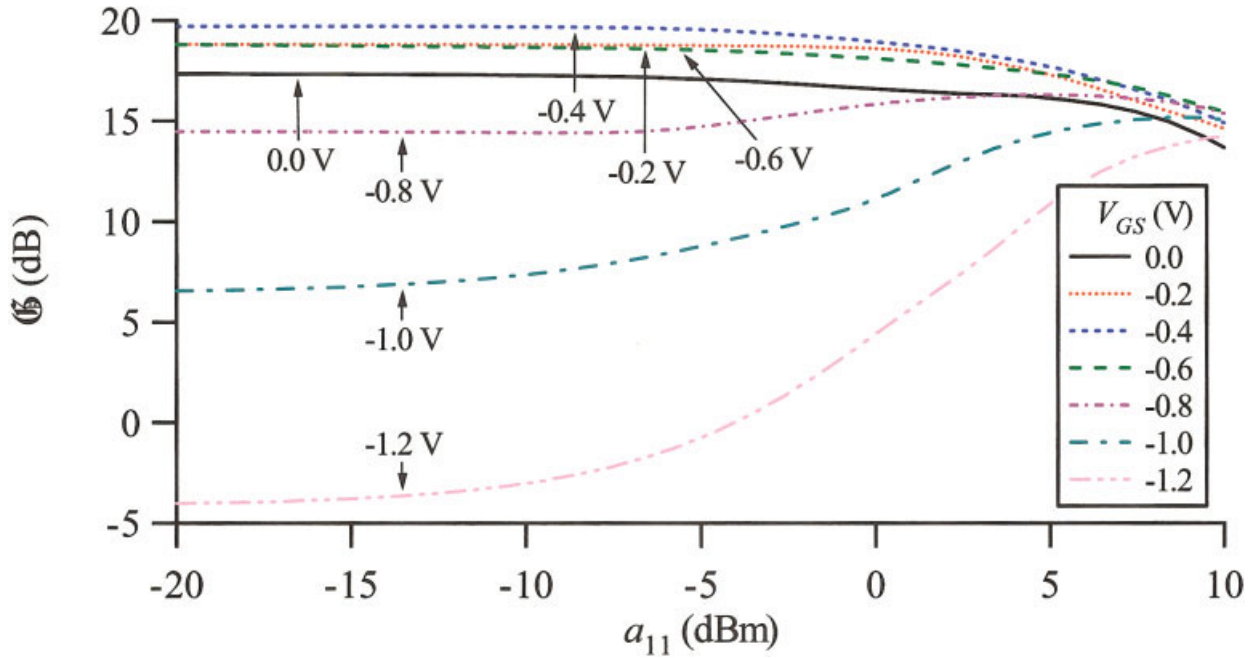
Figure 3. Magnitude of $\mathfrak{S}_{21k1}$ as a function of input power for a nonlinear lumped-element model of a 2×90 μm GaAs pHEMT device operating at 5 GHz and a bias of $V_{DS} = 3$ V and $V_{GS} = 0.0$, -0.2, -0.4, -0.6, -0.8, and -1.0 V.
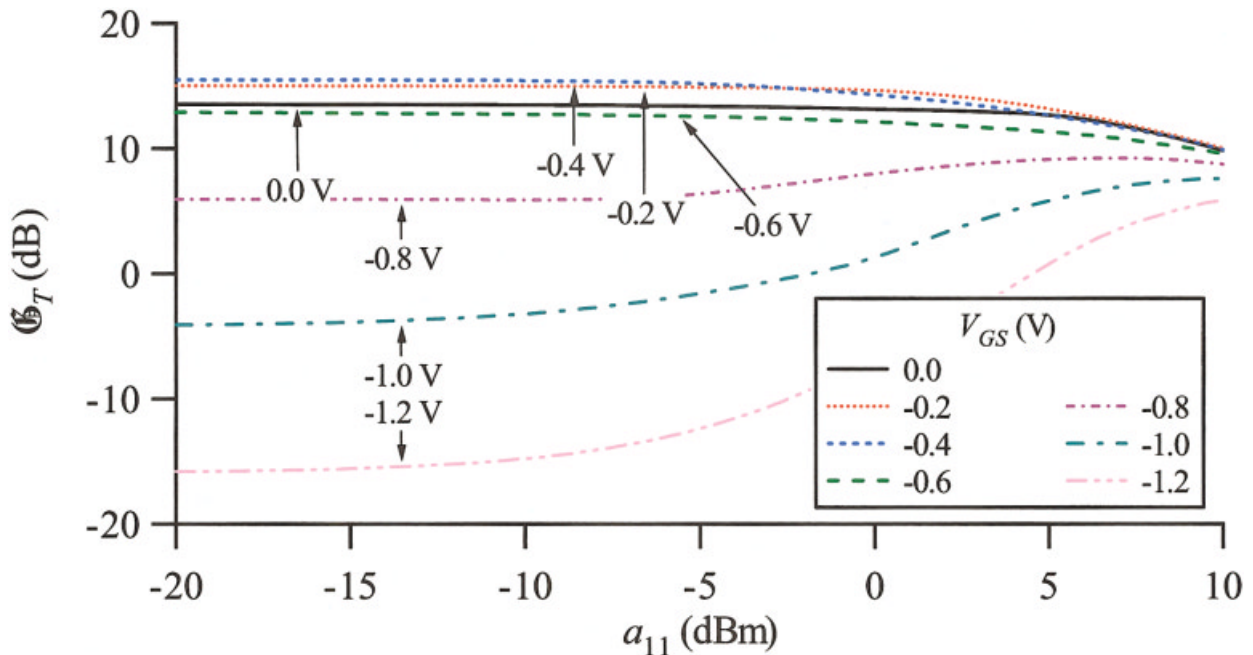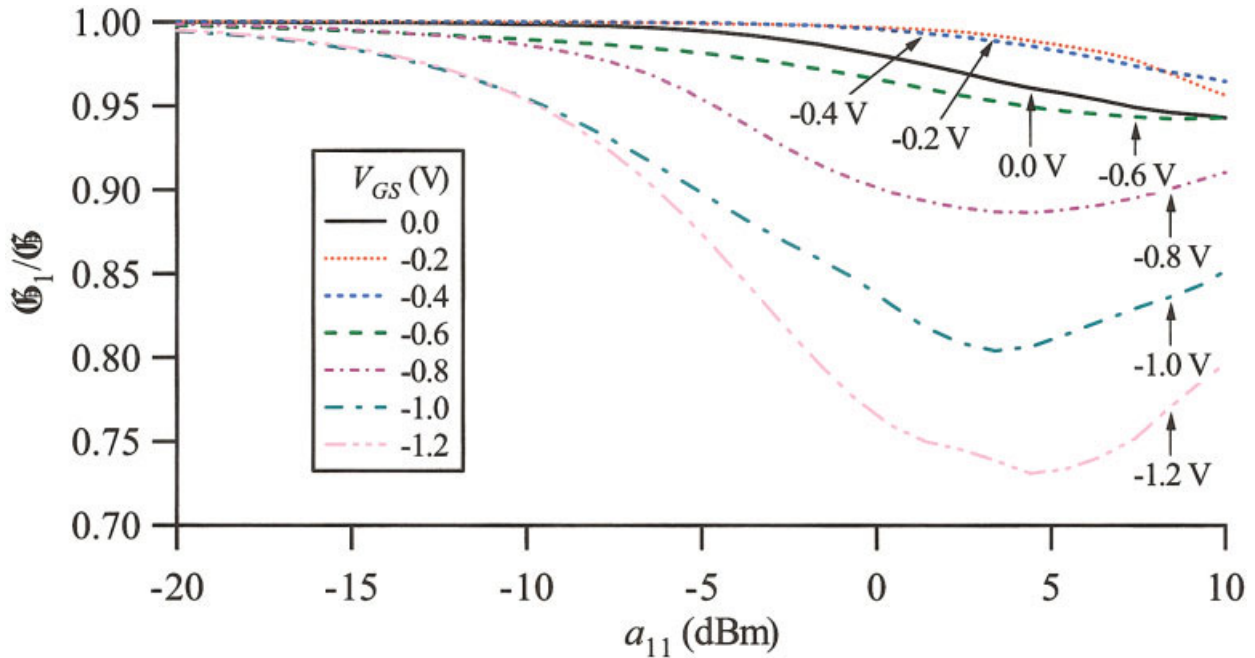
Figure 4. Phase of $\mathbb{S}_{11k1}$ and $\mathbb{S}_{21k1}$ as a function of input power for a nonlinear lumped-element model of a 2×90 μm GaAs pHEMT device operating at 5 GHz and a bias of $V_{DS} = 3$ V and $V_{GS} = 0.0$, -0.4, and -1.0 V.

Figure 5. Expanded power gain $\mathcal{G}$ as a function of input power for a nonlinear lumped-element model of a 2×90 μm GaAs pHEMT device operating at 5 GHz and a bias of $V_{DS} = 3$ V and V_{GS} = 0.0, −0.2, −0.4, −0.6, −0.8, −1.0, and −1.2 V. [Color figure can be viewed in the online issue, which is available at www.interscience.wiley.com.]

Figure 6. Expanded transducer gain $\mathcal{G}_T$ as a function of input power for a nonlinear lumped-element model of a 2×90 μm GaAs pHEMT device operating at 5 GHz and a bias of $V_{DS} = 3$ V and $V_{GS} = 0.0$, −0.2, −0.4, −0.6, −0.8, −1.0, and −1.2 V. [Color figure can be viewed in the online issue, which is available at www.interscience.wiley.com.]

Figure 7. The ratio $\mathcal{G}_1/\mathcal{G}$ as a function of input power for a nonlinear lumped-element model of a 2×90 μm GaAs pHEMT device operating at 5 GHz and a bias of $V_{DS} = 3$ V and $V_{GS} = 0.0$, -0.2, -0.4, -0.6, -0.8, -1.0, and -1.2 V. [Color figure can be viewed in the online issue, which is available at www.interscience.wiley.com.]

reaches a maximum of 15.48 dB at $V_{GS} = -0.4$ V, and then decreases as V_{GS} is further decreased from -0.4 V to -1.2 V. And, similar to power gain, the transducer gain stays relatively flat and then gradually decreases with increasing $|a_{11}|$ for values of V_{GS} from 0 V to -0.6 V. At V_{GS} less than -0.6 V, the transducer gain increases with increasing $|a_{11}|$ due to self-biasing and harmonic production.

Comparing the plots of power gain and transducer gain in Figures 5 and 6, we can see that the values of transducer gain are less than those of power gain, due to the large values of $\mathcal{S}_{1111}$ which inflate the values of power gain. Another difference to note is that the power gain at $V_{GS} = -0.4$ V is always greater than at $V_{GS} = -0.2$ V, but the transducer gain at $V_{GS} = -0.4$ V is only greater than at $V_{GS} = -0.2$ V up to $|a_{11}| = -2.6$ dBm. At higher input powers, the transducer gain is slightly higher at $V_{GS} = -0.2$ V than at $V_{GS} = -0.4$ V.

Figure 7 plots the ratio of the power gain confined to the first harmonic to that of the overall power gain, $\mathcal{G}_1/\mathcal{G}$. Recall that $\mathcal{G}_1/\mathcal{G} = \mathcal{G}_{T1}/\mathcal{G}_T$. At small signals, $\mathcal{G}_1/\mathcal{G}$ is relatively high for all values of V_{GS}, but is at a maximum of 0.9958 for $V_{GS} = -0.4$ V. As $|a_{11}|$ increases, $\mathcal{G}_1/\mathcal{G}$ remains relatively high for V_{GS} at

-0.2 V and -0.4 V. At V_{GS} less than -0.4 V, $\mathcal{G}_1/\mathcal{G}$ decreases dramatically with increasing $|a_{11}|$ since much of the energy in the device is converted to higher harmonic frequencies. In fact, at $V_{GS} = -1.2$ V, $\mathcal{G}_1/\mathcal{G}$ drops to 0.731.

From Figures 5, 6, and 7, we can clearly see that the optimum gate-to-source bias condition is near $V_{GS} = -0.4$ V for the device at $V_{DS} = 3$ V, where $\mathcal{G}$, $\mathcal{G}_T$, and $\mathcal{G}_1/\mathcal{G}$ are highest. Furthermore, if we look at the power gain at this particular bias condition, shown in Figure 8, we find the 1-dB gain compression point to be $\mathcal{G}_{1dB} = 18.716$ dB, which occurs at $|a_{11}| = 1.40$ dBm.

Also shown in Figure 8 is the traditional power gain G. For this example, where a_{11} is the only incident wave present, G can be expressed in terms of nonlinear large-signal scattering parameters as:

$$G = \frac{|\mathcal{S}_{2111}|^2}{1 - |\mathcal{S}_{1111}|^2}. \tag{26}$$

We see from Figure 8 that at small input signals $\mathcal{G}$ and G are nearly identical, but at higher powers $\mathcal{G}$ is greater than G since the traditional power gain does
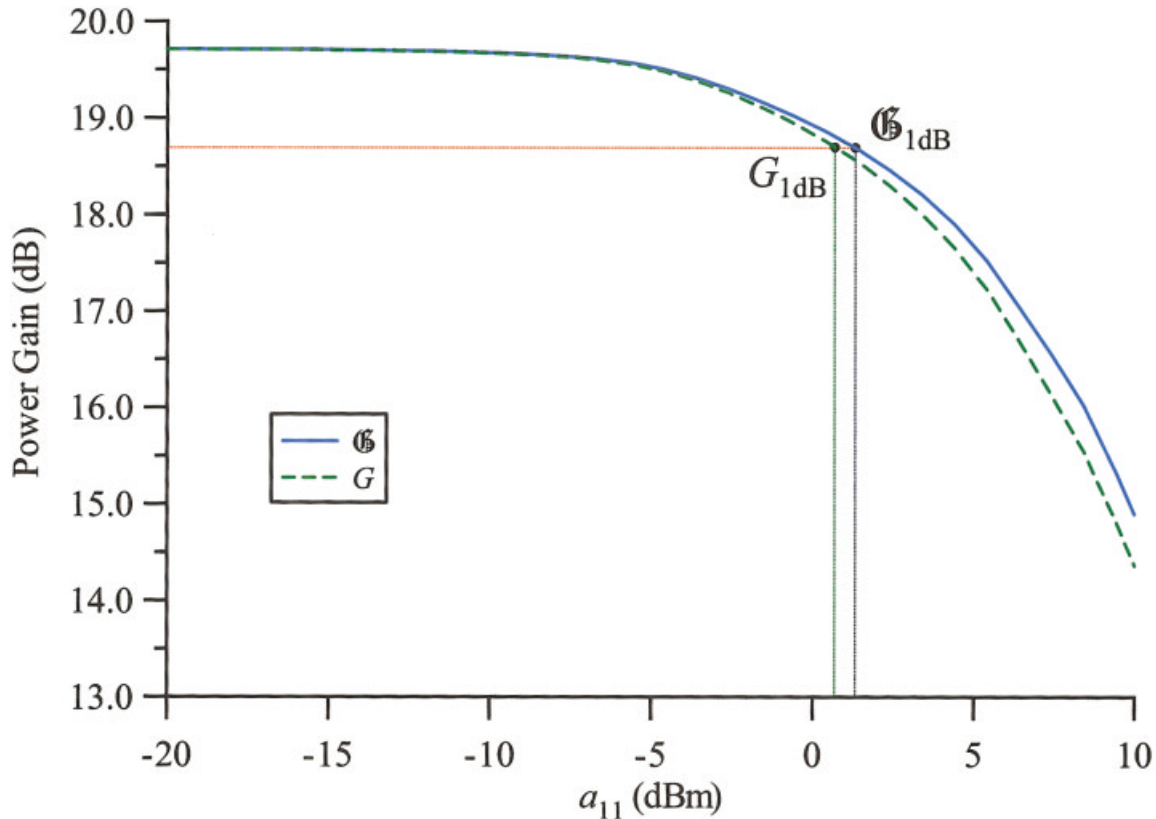
Figure 8.   The 1-dB gain compression point for a nonlinear lumped-element model of a $2 \times 90\ \mu$m GaAs pHEMT device operating at 5 GHz and a bias of $V_{DS} = 3$ V and $V_{GS} = -0.4$ V. [Color figure can be viewed in the online issue, which is available at www.interscience.wiley.com.]

not take into account the power generated at higher harmonic frequencies. Using G, we get the same 1-dB gain compression point of $G_{1\text{dB}} = 18.716$ dB, but it occurs at $|a_{11}| = 0.78$ dBm.

V. CONCLUDING REMARKS

We expanded the definitions of power gain, transducer gain, and available gain by taking harmonic content into account, and showed that under special conditions, this generalized power gain can be expressed in terms of nonlinear large-signal scattering parameters. We provided an example showing how the expanded definitions of gain and nonlinear large-signal scattering parameters can be used to examine the behavior of a nonlinear model by simply performing a harmonic-balance simulation with all a's other than a_{11} forced to zero. Looking at the nonlinear large-signal scattering parameters has given us an in-depth view of the modeled behavior by allowing us to separate out the input reflection coefficients and

transmission coefficients for each of the frequency components, while reducing the nonlinear large-signal scattering parameter data set into the compact expressions of power gain $\mathfrak{G}$, transducer gain $\mathfrak{G}_T$, and the ratio $\mathfrak{G}_1/\mathfrak{G}$, thus giving us a more concise view of the modeled behavior.

Although we generated nonlinear large-signal scattering parameters by performing a harmonic-balance simulation with all a's other than a_{11} forced to zero, it is important to note that we can extract these parameters indirectly through measurements. In references [2–3], we have shown a method for doing this. Specifically, we trained an artificial neural network (ANN) with multiple measurements made on a device using a nonlinear vector network analyzer [7–8] equipped with a second source. Once the ANN was trained, we extracted the nonlinear large-signal scattering parameters by interpolating from the measured results for nonzero values of a_{mn} $[(m \neq 1) \wedge (m \neq 1)]$ to the desired values for a_{mn} $[(m \neq 1) \wedge (m \neq 1)]$ equal to zero.

ACKNOWLEDGMENTS

REFERENCES

1. D.M. Pozar, Microwave engineering, 2nd ed., Wiley, New York, 1997.

2. J.A. Jargon, K.C. Gupta, D. Schreurs, K.A. Remley, and D.C. DeGroot, A method of developing frequency-domain models for nonlinear circuits based on large-signal measurements, 58th ARFTG Conf Dig, San Diego, CA, 2001, pp. 35–48.

3. J.A. Jargon, K.C. Gupta, D. Schreurs, and D.C. De-Groot, Developing frequency-domain models for nonlinear circuits based on large-signal measurements, Proc XXVIIth General Assembly Int Union Radio Sci, CD-ROM A1.O.6, Maastricht, The Netherlands, 2002.

4. J.A. Jargon, D.C. DeGroot, K.C. Gupta, and A. Cidronali, Calculating ratios of harmonically related, complex signals with application to nonlinear large-signal scattering parameters, 60th ARFTG Conf Dig, Washington, D.C., 2002, pp. 113–122.

5. A. Cidronali, G. Collodi, A. Santarelli, G. Vannini, and G. Manes, Millimeter-wave FET modeling using on-wafer measurements and EM simulation, IEEE Trans Microwave Theory Tech 50 (2002), 425–432.

6. A. Cidronali, G. Collodi, C. Toccafondi, R. Cignani, A. Santarelli, G. Vannini, and F. Filicori, A distributed approach for the characterization of parasitic networks in electron device modeling, GAAS 2002, Milan, Italy, 2002, pp. 149–152.

7. J. Verspecht, P. Debie, A. Barel, and L. Martens, Accurate on wafer measurement of phase and amplitude of the spectral components of incident and scattered voltage waves at the signal ports of a nonlinear microwave device, 1995 IEEE MTT-S Int Microwave Symp Dig, vol. 3, 1995, pp. 1029–1032,

8. J. Verspecht, Calibration of a measurement system for high-frequency nonlinear devices, doctoral dissertation, Vrije Universiteit, Brussels, Belgium, 1995.

BIOGRAPHIES

Jeffrey A. Jargon received B.S. and M.S. degrees in electrical engineering from the University of Colorado at Boulder in 1990 and 1996, respectively. He has been with the Radio Frequency Technology Division, National Institute of Standards and Technology (NIST), Boulder, CO, since 1990. His current research interests include calibration techniques for vector network analyzers and artificial neural network modeling of passive and active devices. He has authored or co-authored more than 30 technical publications and conference presentations, and received two best paper awards. He is a member of Tau Beta Pi and Etta Kappa Nu, a Senior Member of IEEE, and is a registered Professional Engineer in the State of Colorado. He is currently pursuing his Ph.D. degree in electrical engineering at the University of Colorado at Boulder.

K. C. Gupta has been a Professor at the University of Colorado since 1983. Presently, he is also the Associate Director for the NSF I/UCR Center for Advanced Manufacturing and Packaging of Microwave, Optical and Digital Electronics (CAMP-mode) at the University of Colorado, and a Guest Researcher with the RF Technology Group of the National Institute of Standards and Technology (NIST) at Boulder. He received B.E. and M.E. degrees in Electrical Communication Engineering from the Indian Institute of Science, Bangalore, India, in 1961 and 1962, respectively, and his Ph.D. degree from the Birla Institute of Technology and Science, Pilani, India, in 1969. His current research interests are in the area of computer-aided design techniques (including ANN applications) for microwave and millimeter-wave integrated circuits, nonlinear characterization and modeling, RF MEMS, and reconfigurable antennas. He is the author or co-author of eight books, including Microstrip Line and Slotlines (Artech House, 1979; revised second edition, 1996); CAD of Microwave Circuits (Artech House, 1981; Chinese Scientific Press, 1986; Radio I Syvaz, 1987); Microstrip Antenna Design (Artech House, 1988); and Neural Networks for RF and Microwave Design (Artech House 2000). Also, he has contributed chapters to the Handbook of Microstrip Antennas (Peter Peregrinus, 1989); the Handbook of Microwave and Optical Components, vol. 1 (Wiley, 1989); Microwave Solid State Circuit Design (Wiley, 1988); Numerical Techniques for Microwave and Millimeter Wave Passive Structures (Wiley, 1989), and Encyclopedia of Electrical and Electronics Engineering (Wiley, 1999). He has published about 200 research papers and holds four patents in the microwave area. He is a Fellow of the IEEE, a Fellow of the Institution of Electronics and Telecommunication Engineers (India), a Member of URSI (Commission D, USA), and a Member of the Electromagnetics Academy (MIT, USA). He is a recipient of IEEE-MTTS Distinguished Educator Award, IEEE Third Millennium Medal, a member of the ADCOM for the MTT Society of IEEE, chair of the IEEE MTT-S standing committee on Education, past co-chair of the IEEE MTT-S Technical Committee on CAD (MTT-1), a member of the IEEE Technical Committee on Microwave Field Theory (MTT-15), a member of IEEE-EAB Committee on Continuing Education, a member of IEEE-EAB Societies Education Committee, and on the Technical Program Committees for MTT-S International Symposia. He is the founding editor of the International Journal of RF and Microwave Computer-Aided Engineering, published by Wiley

since 1991. He is an Associate Editor for IEEE Microwave Magazine, on the editorial boards of IEEE Transactions on Microwave Theory and Techniques, Microwave and Optical Technology Letters (Wiley), and International Journal of Numerical Modeling (Wiley, U.K.). He is listed in Who's Who in America, Who's Who in the World, Who's Who in Engineering, and Who's Who in American Education.

Alessandro Cidronali was born in Florence, Italy, in 1965. He received Laurea and Ph.D. degrees in electronic engineering from the University of Florence, Florence, Italy, in 1992 and 1998, respectively. In 1993, he joined the Department of Electronics Engineering, University of Florence, where he became an Assistant Professor in 1999. During his academic career, he has been a lecturer in courses of Applied Electronics and Solid State Electronics and he now teaches Microwave Electronics. His research activities cover the study of active and passive compact structures for monolithic microwave ICs (MMICs), the design of multifunction MMICs for low-power wireless applications, CAD, and numerical modeling of HEMTs for microwave and high-speed applications. He is currently working on basic research on quantum functional devices and their applications to microwave circuits.

Donald C. DeGroot received his Bachelors degree in Electronics Engineering from Andrews University in 1985, and M.S. and Ph.D. degrees in Electrical Engineering from Northwestern University in 1990 and 1993, respectively. Currently, he is the Project Leader with the NIST Nonlinear Device Characterization Project. His present research activities include development of large-signal broadband measurement and calibration techniques for the development and validation of nonlinear circuits. Concurrently, he is Professor Adjoint of Electrical and Computer Engineering at the University of Colorado at Boulder. Prior to joining the RF Electronics Group, he researched and developed microwave superconducting devices and thin film measurements as a National Research Council Postdoctoral Associate at NIST; studied the high-frequency properties of novel electronic materials at Northwestern University; and designed high-speed instrumentation at Fermi National Accelerator Laboratory. He has authored or coauthored numerous technical publications and conference presentations, receiving ARFTG Best Paper and Best Poster Paper awards and an URSI Young Investigator Award. He is a Senior Member of IEEE, participating in professional conference and events committees.